

A Theoretical Model for the Increases in Cutting Edge Recessions During Milling of Nine Species of Wood

Bolesław Porankiewicz,^{a,*} Daria Wieczorek,^b Anita Bocho-Janiszewska,^c
Emilia Klimaszewska,^c Chiaki Tanaka,^d and Wayan Darmawan^e

The high-speed steel (HSS) cutting tool edge recession increase (ΔVB) from milling wood of nine wood species with very different properties were analyzed. Theoretical simulations showed that the synergistic effect of the wood density (D), hard mineral contamination (HMC), and high temperature tribochemical reactions (HTTR), as well as initial edge recessions were important factors that accelerated wearing on the examined cutting edges.

Keywords: Cutting edge recession; High speed steel; Wood; Milling; High temperature tribochemical reactions

Contact information: a: LAB-TECH, 97-500 Radomsko, ul. Krasickiego 13, Poland; b: Poznań University of Economics and Business, Faculty of Commodity Science, Department of Technology and Instrumental Analysis, 61-875 Poznań, al. Niepodległości 10, Poland; c: Department of Chemistry, University of Technology and Humanities in Radom 26-600 Radom, ul. Chrobrego 27, Poland; d: Emeritus, PhD, Professor; e: Department of Forest Products, Faculty of Forestry, Bogor Agricultural University (IPB), Bogor 16680, Indonesia; *Corresponding author: poranek@amu.edu.pl

INTRODUCTION

Wood cutting tool edge wearing and the role of the high temperature tribochemical reactions (HTTR) and hard mineral contaminations (HMC) during wearing has not been fully explained nor quantified. Cristóvão *et al.* (2009) and Cristóvão *et al.* (2011) are good examples of recent works in which the dulling of fast cutting tools after machining wood specimens from tropical forests was associated mainly with large HMC, but the influence of the HTTR and the size of the HMC particles were not taken into account, despite several publications on this subject (Porankiewicz *et al.* 2005, 2006, 2008). The fast wearing of cutting tools in the cited works was attributed not only to the HMC, the HTTR, and the size of the HMC particles, but also to the synergistic effect of chemical and mechanical factors on wear. Another reason for this problem, which has not been solved yet, is the limited amount of wood specimens examined. Recent repetitions of the thermal gravimetry analysis (TGA) for several solid wood species originating from Indonesia and Japan, together with carbonyl iron powder, show major differences in comparison to results of tests reported in previous works (Porankiewicz *et al.* 2005, 2006, 2008), so there is a presumption that this diversity may not be related to properties of examined wood specimens. In the present work the mechanism of the HSS tool cutting edge recessions after longitudinal milling, reported in previous experiments (Porankiewicz *et al.* 2005, 2006, 2008), were reanalyzed. Of the HMC, the HTTR and the density (D), and some mechanical properties of wood specimens that were examined, some were very small and some very great.

EXPERIMENTAL

Machine tests were performed by Dr. Jakub Sandak and Dr. Piotr Iskra in the laboratory of Shimane University, Matsue, Japan, using a Shoda FANUC NC-3 computer numerical controlled machine (Hamamatsu, Shizuoka, Japan; Fig. 1) under the following machining conditions: rotation speed of a spindle (n), 2,864 min^{-1} ; cutting speed (v_C), 30 m/s; number of cutting edges (z), 1; feed rate per tooth (f_Z), 0.1 mm; rake angle (γ_F), 30°; sharpness angle (β_F), 55°; cutting depth (g_S), 1.5 mm; and moisture content (m_C), 11%. The materials of the cutting edge SKH51 were according to JIS G64403. The hardness of the cutting edge material was 64 HRC.

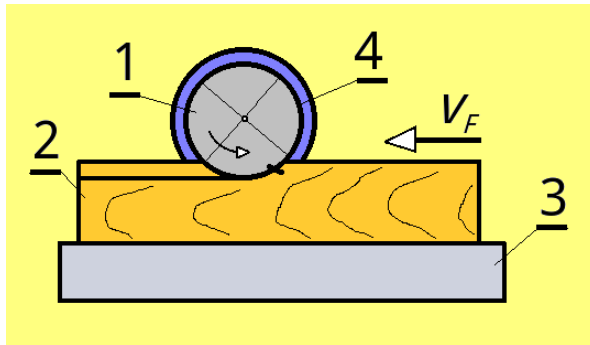


Fig. 1. Cutting machine diagram. 1) cutting tool, 2) working piece, 3) machine table, and 4) electrical motor

The main properties of wood specimens of nine wood specimens are shown in Tables 1 and 2. Images of sections perpendicular to grains are shown in Fig. 2.

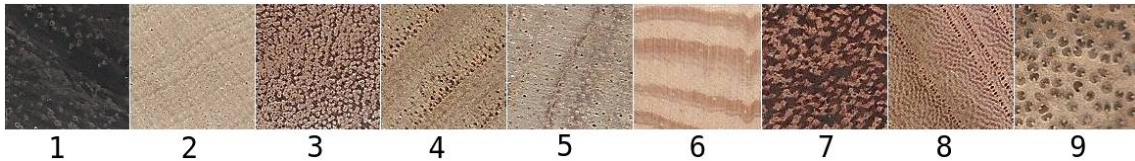


Fig. 2. Scan of sections perpendicular to grains of wood specimens examined: 1 - Ebony; 2 - Hornbeam; 3 - Keirung; 4 - Tamo; 5 - Yellow Meranti; 6 - Japanese Douglas Fir; 7 - Kempas; 8 - Keyaki; 9 - Oilpalm

Table 1. Wood Specimens Examined

| no. | Name | Name | Country of origin |
|-----|---------------------------------|-------------------------------|-------------------|
| 1 | Ebony | <i>Diospyros celebica</i> | Indonesia |
| 2 | Hornbeam; Shide | <i>Carpinus sp.</i> | Japan |
| 3 | Keirung | <i>Combretocarpus sp.</i> | Indonesia |
| 4 | Tamo | <i>Sassafras albidum</i> | Japan |
| 5 | Yellow Meranti | <i>Shorea fauetiana</i> | Indonesia |
| 6 | Japanese Douglas Fir; Kuromatsu | <i>Pseudotsuga douglasii</i> | Japan |
| 7 | Kempas | <i>Koompassia malaccensis</i> | Indonesia |
| 8 | Keyaki | <i>Zelkova serrata</i> | Japan |
| 9 | Oilpalm | <i>Elaeis guineensis</i> | Indonesia |

Table 2. Mechanical Properties of Wood Specimens Examined

| no. | <i>D</i> | <i>MOR</i> | <i>E</i> | <i>CS</i> |
|-----|----------|------------|----------|-----------|
| 1 | 1,030 | 115.2 | 15.29 | 62.6 |
| 2 | 710 | 110.4 | 12.10 | 50.5 |
| 3 | 698 | 121.1 | 14.17 | 61.9 |
| 4 | 520 | 74.6 | 8.24 | 25.7 |
| 5 | 460 | 91.7 | 10.40 | 53.0 |
| 6 | 553 | 66.0 | 11.30 | 43.0 |
| 7 | 880 | 138.7 | 21.71 | 75.1 |
| 8 | 706 | 97.4 | 11.76 | 50.1 |
| 9 | 395 | 36.1 | 4.59 | 4.3 |

D - (kg·m⁻³), *MOR* - Modulus of Rupture by Bending (MPa), *E*- Modulus of Elasticity (GPa), *CS*- Compression Strength (MPa)

For the estimation of the HTTR of products of thermal degradation of wood towards iron, a method based on the TGA was used, as described in earlier works (Porankiewicz 2003a; 2003b). The HTTR peaks were recognized as a rapid mass (*m*) increased on a first derivative (dm/dt) of the *m* against time, *t* (min) plots (dTG). Figure 3 shows peaks of the HTTR. For the characterization of the HTTR of products of thermal decomposition of wood and iron, a binder of the cutting edge material, the following quantifiers were examined: *R_{MX}* - maximum; *R_{MI}* - minimum; *R_{Xs}* - average of three maximums; *R_{Ws}* - average of weights according to temperature of maximum, *T_X*; *R_{As}* - average of maximum corrosion peaks area; *R_{Ss}* - average of all corrosion peaks. These quantifiers were calculated according to Eqs. 1 through 6,

$$R_{MX} = r_{xj} \cdot m^{-1} \quad (\text{min}^{-1}) \quad (1)$$

$$R_{MI} = r_{ij} \cdot m^{-1} \quad (\text{min}^{-1}) \quad (2)$$

$$R_{Xs} = \Sigma(r_{xi} \cdot m^{-1}) \cdot 3^{-1} \quad (\text{min}^{-1}) \quad (3)$$

$$R_{Ws} = \Sigma[(r_{xj} \cdot T_{xj}) \cdot m^{-1}] \cdot (3 \cdot \Sigma T_{xj})^{-1} \quad (\text{min}^{-1}) \quad (4)$$

$$R_{As} = \Sigma A_{ij} \cdot 3^{-1} \quad (\text{mg} \cdot 1^0 \cdot \text{min}^{-1}) \quad (5)$$

$$R_{Ss} = \Sigma[\Sigma(r_{ij} \cdot m^{-1}) \cdot n_j^{-1}] \cdot 3^{-1} \quad (\text{min}^{-1}) \quad (6)$$

where *m* is the mass of iron powder specimen (mg); *r_{xj}* and *T_{xj}* are, respectively, the maximum height and temperature of corrosion peak after maximum mass degradation (point *M* in Fig. 3) in repetition *j* (mg/min); *r_{ij}* is the maximum height corrosion peak indexed by *i* (including peaks before and after point *M* in Fig. 3) in the repetition *j* (mg/min); *A_{ij}* is the area of corrosion peak indexed as *i* (including peaks before and after point *M*) in the repetition *j* (Fig. 3); *j* is the index for the repetition; *n_j* is the number of corrosion peaks taken into account in one repetition *j*. The number of TGA repetitions performed was *j* = 3.

The *R_{Xs}*, the *R_{MX}*, the *R_{MI}*, and the *R_{Ss}* quantifiers, according to Eqs. 1 through 3 and 6, appear as the relative speed of the *Fe* specimen mass increase in the corrosion peaks. For the evaluation of the *R_{Xs}*, the *R_{MX}*, the *R_{MI}*, *R_{Ws}*, and *R_{As}* quantifiers, corrosion peaks in the temperature range of 276 °C to 309 °C were taken into account. For quantifier *R_{Ss}*

corrosion peaks were also taken into account, before and after point *M* in Fig. 3, which were from 202 °C to 223 °C and from 395 °C to 416 °C, without small peaks (narrow and short), marked in Fig. 3 as 'S'.

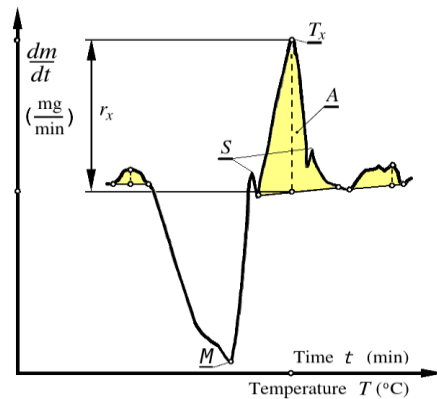


Fig. 3. Parameters of the corrosion peak used for calculations of the quantifier, R_{MX} ; dm/dt - first derivative of mass, m (mg), against time, t (min); r_x - height of corrosion peak (mg/min); T_x - temperature of maximum corrosion peak (°C); A - area of corrosion peak

For the evaluation of the content of the HMC of wood specimens, a combustion method was applied (Porankiewicz 2003a,b; Porankiewicz *et al.* 2005, 2006). The crucibles with the ash and black particles of coal that were not burned completely were kept in a muffle oven at a temperature of 470 °C. This temperature was lower than in previous analyses so that the ash would not melt, in the case of a higher content of the potassium (K). Such a situation might result in the creation of silica particle aggregates, which had happened in a previous work (Porankiewicz *et al.* 2005). The combustion method was also expanded by the additional burning of the millipore glass-fiber filters at a temperature of 350 °C, as long as it was needed for black particles of charcoal to disappear. In the present study the average values of the content of the HMC from actual and previous studies were taken into account. Residues on the glass-fiber filters were examined using a scanning electron microscope (SEM). The solutions of filtrates of salt acid after digestion of ash were analyzed using energy dispersive spectroscopy (EDAX); the surface was analyzed for elemental and semiquantitative properties of calcium (Ca), potassium (K), sodium (Na), magnesium (Mg), and alumina (Al). The EDAX was also employed for analysis of hard contamination particles.

The cutting edge recession measured: VB_S , the clearance surface; VB_W , bisector of wedge angle; and VB_F , the rake surface (Fig. 4). The cutting edge profiles were scanned under vertical magnification of $\times 50$, with the use of a stylus, perpendicular to the edge, in three paths, separated by 1 mm. The theoretical model developed is described by Eqs. 7 through 31 (Porankiewicz 2006). The predicted cutting edge recession, VB^P , was defined by Eq. 7. The summation of the elementary wearing effects ΔVB_{1ij} and ΔVB_{2ijk} along the cutting arc and the total feed path is given by $L_{F1-4} = 86,245$ mm for specimens nos. 1-4, whereas for specimens nos. 5 to 9 it is $L_{F5-9} = 114,993$ mm. The assumed number of fractions of the HMC was $n_f = 6$, as shown in Table 3. The cutting blade was moved for as many as $n_{cp} = 862,453$ steps for specimens nos. 1 to 4 and $n_{cp} = 1,149,938$ steps for specimens nos. 5 to 9, along the total feed paths L_{F1-4} or L_{F5-9} . The blade was moved n_ϕ steps, along one single cutting arc of length 17.39 mm, from the beginning angle position $\phi_L = -0.0005$ rad to the end angle position of $\phi_U = 0.17342$ rad, inside one feed step of $f_Z = 0.1$ mm.

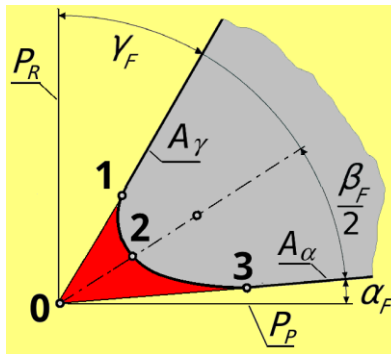


Fig. 4. The parameters of worn cutting edge; 0-1 - VB_F cutting edge recession measured along the rake surface; 0-2 - VB_W cutting edge recession measured along the bisector of wedge angle; 0-3 - VB_S cutting edge recession measured along the clearance surface; A_γ - rake surface; A_α - clearance surface; P_R - face (main) plain; P_P - back plain; γ_F - contour rake angle; α_F - contour clearance angle; β_F - contour wedge angle

$$VB^P = VB_0 + \sum_{i=1}^{i=ncp} \sum_{j=1}^{j=n\phi} \sum_{k=1}^{k=nf} (\Delta VB_{1ij} + \Delta VB_{2ijk}) \leq VB_{MX}^O \text{ (}\mu\text{m)} \quad (7)$$

$$\Delta VB_1 = \Delta VB \cdot qd_{VB} \cdot q_{1R} \cdot q_{1DR} \quad (8)$$

$$\Delta VB_1 = e_1 \cdot C_{Pi}^{e_2} - e_1 \cdot (C_P - \Delta C_{Pi-1})^{e_2} \quad (9)$$

$$qd_{VB} = e_3 \cdot e_W^{-e_4 - \ln(VB) + e_5} \quad (10)$$

$$q_{1R} = 1 + e_7 \cdot R^{e_8} \text{ for } VB^P > e_6 \quad (11)$$

$$q_{1DR} = 1 + e_{22} \cdot D^{e_{23}} \quad (12)$$

$$\Delta VB_{2f1} = we_{2f1} \cdot S_{f1} \cdot qd_{VB} \cdot q_{2Rf1} \cdot q_{2DR} \quad (13)$$

$$\Delta VB_{2f2} = we_{2f2} \cdot S_{f2} \cdot qd_{VB} \cdot q_{2Rf2} \cdot q_{2DR} \quad (14)$$

$$\Delta VB_{2f3} = we_{2f3} \cdot S_{f3} \cdot qd_{VB} \cdot q_{2Rf3} \cdot q_{2DR} \quad (15)$$

$$\Delta VB_{2f4} = we_{2f4} \cdot S_{f4} \cdot qd_{VB} \cdot q_{2Rf4} \cdot q_{2DR} \quad (16)$$

$$\Delta VB_{2f5} = we_{2f5} \cdot S_{f5} \cdot qd_{VB} \cdot q_{2Rf5} \cdot q_{2DR} \quad (17)$$

$$\Delta VB_{2f6} = we_{2f6} \cdot S_{f6} \cdot qd_{VB} \cdot q_{2Rf6} \cdot q_{2DR} \quad (18)$$

$$q_{2Rf1} = 1 + e_{10} \cdot R^{e_9} \text{ for } VB^P > e_6 \quad (19)$$

$$q_{2Rf2} = 1 + e_{11} \cdot R^{e_9} \text{ for } VB^P > e_6 \quad (20)$$

$$q_{2Rf2} = 1 + e_{12} \cdot R^{e_9} \text{ for } VB^P > e_6 \quad (21)$$

$$q_{2Rf2} = 1 + e_{13} \cdot R^{e_9} \text{ for } VB^P > e_6 \quad (22)$$

$$q_{2Rf2} = 1 + e_{14} \cdot R^{e_9} \text{ for } VB^P > e_6 \quad (23)$$

$$q_{2Rf2} = 1 + e_{15} \cdot R^{e_9} \text{ for } VB^P > e_6 \quad (24)$$

$$q_{Sf1} = e_{16} \cdot f_1 \quad (25)$$

$$q_{Sf2} = e_{17} \cdot f_2 \quad (26)$$

$$q_{Sf3} = e_{18} \cdot f_3 \quad (27)$$

$$q_{Sf4} = e_{19} \cdot f_4 \quad (28)$$

$$q_{Sf5} = e_{20} \cdot f_5 \quad (29)$$

$$q_{Sf6} = e_{21} \cdot f_6 \quad (30)$$

$$q_{2DR} = 1 + e_{24} \cdot D^{e_{25}} \quad (31)$$

where VB_0 is the initial edge recession; VB^P is the predicted recession along the clearance

surface, along the bisector, and along the rake face which are, respectively, VB^P_F , VB^P_W , and VB^P_S ; ΔVB_I is the VB^P increase due to frictional contact with wood; $we_{2fk} \cdot S_{fk}$ is the predicted recession, VB^P , effect related to the action of a single HMC particle, from its position against the edge for fraction f_k ; q_{dvb} is the quotient for the slow down effect of VB^P with the increase of the VB^P ; q_{1R} is the quotient of increase of the VB^P due to HTC expressed by R quantifiers; the q_{1DR} is the quotient of the increase of the cutting edge recession due to the wood density and the properties taken into account; ΔVB_{2fk} is the VB^P increase because of contact with particles of mineral contamination for fractions f_k ; the q_{2Rfk} is the quotient of increase of the VB^P due to HTTR, expressed by the HTTR quantifiers, together with particles of HMC of fractions nos. 1 - 6; the q_{2DR} is the quotient of increase of the VB^P due to the density and the properties taken into account, together with particles of HMC, $e_W = 2.7182818$.

During the evaluation process, the elimination of unimportant or low important estimators by use of coefficient of relative importance (C_{RI}) defined by Eq. 3, assuming $C_{RI} > 0.1$, was done,

$$C_{RI} = (S_K - S_{K0k}) \cdot S_K^{-1} \cdot 100 (\%) \quad (32)$$

where S_{K0k} is the summation of square of residuals, by estimator $C_k = 0$, and C_k is the estimator no. k in statistical model evaluated. The summation of residuals square, S_K , standard deviation, S_D , and the correlation coefficient of the predicted and observed values, R , were used for characterization of approximate quality. Calculations were performed at Poznań Networking & Supercomputing Center PCSS, on a SGI Altix 3700 computer, using a special optimization program, based on a least squares method combined with gradient and Monte Carlo methods developed by the author.

RESULTS AND DISCUSSION

Table 3 summarizes the C_{MC} , the content of ash (C_{AS}), as well as the HTTR quantifiers evaluated from TGA plots, shown in Fig. 5. Wood specimen no. 3 had the greatest hard mineral contamination, while 1, 5, 6, and 8 had low levels of contamination. The C_{MC} did not follow the C_{AS} , although the C_{AS} was very high for wood specimens nos. 3 and 9, having the largest C_{MC} . The C_{MC} was as high as 81.5% of the C_{AS} , in case of wood specimen no. 3, while only 0.06% and 0.07% in case of specimen no. 8 and no. 5, respectively. Because of an insufficient amount of wood, evaluation of the dispersion of the HMC was not possible, but this feature of wood species originating from rain forests is large Amos (1952).

Figure 5 shows that corrosion peaks in the temperature range from 276 °C to 309 °C are very large for all of the wood specimens. They were not similar to those reported in previous works (Porankiewicz *et al.* 2005, 2006, 2008). The reason for that remains unknown, probably due to the operator and/or a TGA apparatus error. Low dispersion of the height of corrosion peaks, for three repetitions, can be seen for wood specimens nos. 5 and 7 ($S_D = 0.001 - 0.004$), while for wood specimens nos. 1 and 3 the dispersion was much larger (0.031 - 0.034). The wood specimen no. 7 does not show the HTTR peak in the temperature range from 395 °C to 416 °C. The R_{AS} quantifier was the largest of all for wood specimen no. 6, while the maximum for the other quantifiers can be seen for other species.

Table 3. Content of the HMC, $C_{MC}(\text{mg}\cdot\text{kg}^{-1})$, Content of Ash, $C_{AS}(\%)$, the HTTR Quantifiers $R_{As}(\text{mg}\cdot 1^{\circ}\cdot\text{mgin}^{-1})$, R_{Xs} , R_{Ws} , R_{Ss} , R_{MX} , $R_{MI}(\text{min}^{-1})$

| No. 1 | C_{MC} | C_{AS} | R_{As} | R_{Xs} | R_{Ws} | R_{Ss} | R_{MX} | R_{MI} |
|-------|----------|----------|----------|----------|----------|----------|----------|----------|
| 1 | 47.2 | 0.61 | 2.32 | 0.1013 | 0.1287 | 0.1187 | 0.1198 | 0.0756 |
| 2 | 275.7 | 0.52 | 1.84 | 0.1001 | 0.1139 | 0.115 | 0.1149 | 0.0831 |
| 3 | 12,966 | 1.59 | 1.36 | 0.0847 | 0.0656 | 0.0847 | 0.1119 | 0.0642 |
| 4 | 984 | 0.4 | 1.717 | 0.0947 | 0.0991 | 0.0947 | 0.1039 | 0.0793 |
| 5 | 4.8 | 0.65 | 1.844 | 0.0844 | 0.0999 | 0.0546 | 0.0978 | 0.0751 |
| 6 | 77.2 | 0.59 | 2.354 | 0.085 | 0.1184 | 0.0695 | 0.0971 | 0.0782 |
| 7 | 117.7 | 0.09 | 1.783 | 0.09 | 0.1036 | 0.103 | 0.1036 | 0.064 |
| 8 | 54.8 | 9.32 | 2.293 | 0.0899 | 0.1174 | 0.1149 | 0.1 | 0.076 |
| 9 | 4565.2 | 2.18 | 1.947 | 0.1109 | 0.1194 | 0.1187 | 0.12 | 0.1007 |

Remarks: Average size of the C_{MC} for wood specimens nos. 3, 5, 6, 7, and 9 belongs to f_1 ($0\ \mu\text{m} - 50\ \mu\text{m}$, average $25\ \mu\text{m}$), for specimen no. 1, there were also: $2.1\ \text{mg}\cdot\text{kg}^{-1}$ of fraction f_4 ($100\ \mu\text{m} - 200\ \mu\text{m}$, average $150\ \mu\text{m}$) and $5.7\ \text{mg}\cdot\text{kg}^{-1}$ of fraction f_5 ($200\ \mu\text{m} - 400\ \mu\text{m}$, average $300\ \mu\text{m}$); for specimen no. 2, there were also: $0.4\ \text{mg}\cdot\text{kg}^{-1}$ of fraction f_4 ; for specimen no. 4, there were: $2.5\ \text{mg}\cdot\text{kg}^{-1}$ of fraction f_5 and $29\ \text{mg}\cdot\text{kg}^{-1}$ of fraction f_6 ($400\ \mu\text{m} - 600\ \mu\text{m}$, average $500\ \mu\text{m}$); for specimen no. 8, there were also: $30.9\ \text{mg}\cdot\text{kg}^{-1}$ of fraction f_2 ($50\ \mu\text{m} - 75\ \mu\text{m}$, average $63\ \mu\text{m}$)

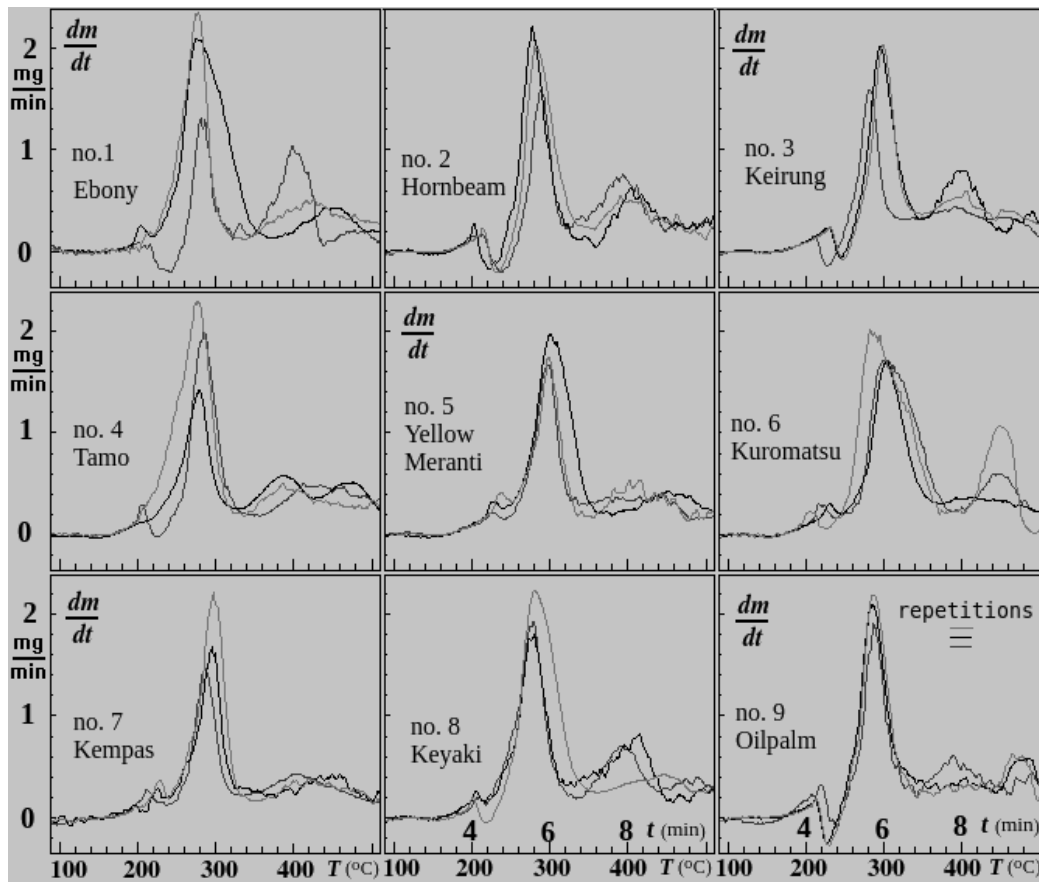


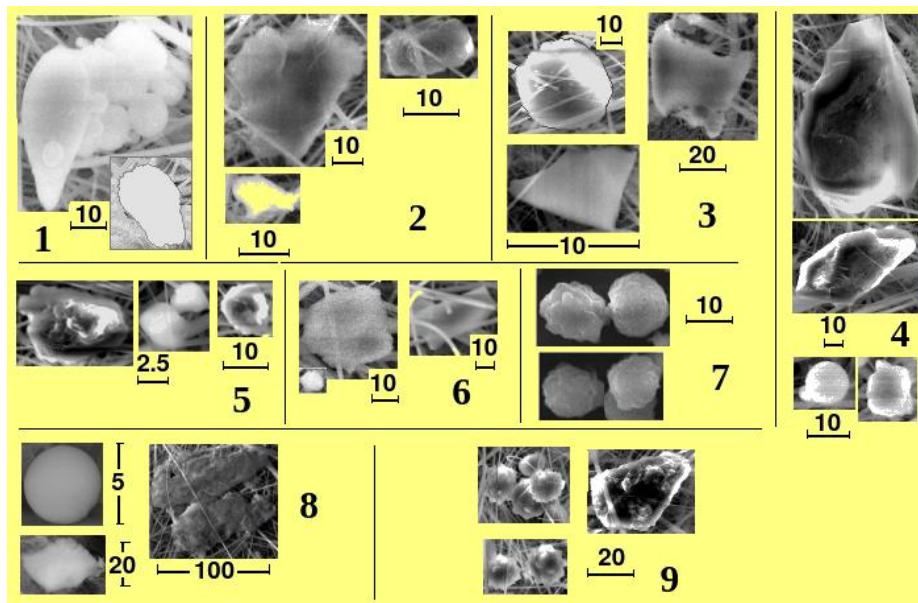
Fig. 5. The TGA (TG and dTG) plots of Fe with wood specimens nos. 1 - 9; t - time, T - temperature

Table 4. Initial Recessions of the Cutting Edge VB_{0F} , VB_{0W} , VB_{0S} (mm) and their Increase DVB_F , DVB_W , DVB_S (mm) after Total Cutting Path Length C_P (m)

| No. | VB_{0F} | VB_{0W} | VB_{0S} | DVB_F | DVB_W | DVB_S | C_P |
|-----|-----------|-----------|-----------|---------|---------|---------|--------|
| 1 | 10.8 | 9 | 10 | 34 | 12 | 12 | 15,000 |
| 2 | 11.7 | 9.4 | 10.3 | 19.8 | 5.1 | 5.1 | 15,000 |
| 3 | 15.9 | 9.9 | 11.0 | 356.6 | 121.1 | 121.1 | 15,000 |
| 4 | 13.7 | 9.4 | 13.7 | 13.3 | 3.1 | 3.1 | 15,000 |
| 5 | 37.7 | 22.7 | 26.2 | 9.2 | 11.8 | 11.7 | 20,000 |
| 6 | 35.2 | 19.8 | 26.2 | 26 | 19.2 | 19.2 | 20,000 |
| 7 | 38.4 | 20.0 | 25 | 14 | 15.8 | 15.8 | 20,000 |
| 8 | 60.5 | 45.0 | 55.7 | 232.3 | 79 | 79 | 20,000 |
| 9 | 33.5 | 24.3 | 38 | 276.9 | 71.1 | 61.1 | 20,000 |

Table 4 summarizes the HSS cutting edge initial recessions VB_0 and the increase of the ΔVB and the total cutting path, C_P . The largest ΔVB for specimen nos. 3 and 9 (Table 4) might be associated with very high C_{MC} ; however specimen no. 8 had both low contamination and a very large cutting edge recession. This observation shows that exceptionally large cutting edge recession cannot be explained only by HMC, as has been done in many published papers, for example Cristóvão *et al.* (2009) and Cristóvão *et al.* (2011), while the HTTR role in the HSS tool wearing process was reported many years ago (Porankiewicz *et al.* 2005, 2006).

Particles of the HMC extracted from wood specimens tested in the actual study are shown in Fig. 6. In the case of all wood specimens, ball alike and irregular particles were found.

**Fig. 6.** Particles of hard mineral contamination extracted from the wood specimens nos. 1 - 9

The size of most particles in wood specimens nos. 3, 5, 6, 7, and 9, was lower than 50 μm . In wood specimens no. 8 (also in nos. 1, 2, and 4 from a previous study (Porankiewicz *et al.* 2005; Porankiewicz *et al.* 2006; Porankiewicz *et al.* 2008)) several larger particles were found in the SEM images. A lack of aggregates of particles in the present combustion analysis of the HMC in all wood specimens was probably due to the lower temperature (470 $^{\circ}\text{C}$) of additional burning of ash in a muffle oven in the present analysis. The surface of particles in the present study seems also to not be coated by a broken glaze, which was reported in earlier works (Porankiewicz *et al.* 2005, 2006).

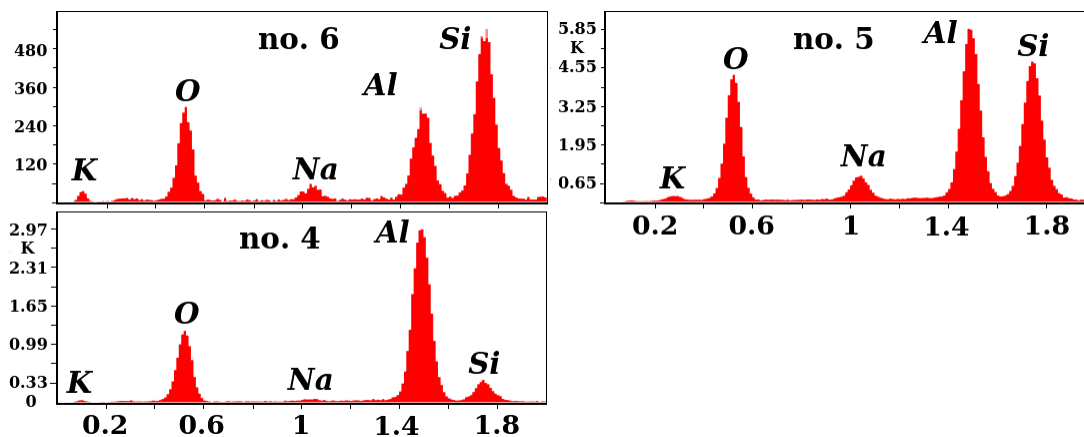


Fig. 7. Plot of EDAX analysis of HMC particles for specimens nos. 4, 5, and 6

Results of the EDAX analysis of the HMC particles (Fig. 7) show that they were Si based, with a small admixture of several other elements (K, Na, Al). However, several particles in the wood specimens nos. 4 and 6 were found to be Al based, without visible impact on the ΔVB . In wood specimen no. 5, HMC particles with high or similar amount of Al and Si were found. In some particles there was evidence of small amounts of other elements (Fe, Br, F, Zn). Results of the EDAX analysis of solution of filtrates show a dominant amount of Ca in wood specimens nos. 1, 3, 4, 5, 7, and 9. The dominant amount of Mg was evidenced in wood specimens nos. 2 and 6, and dominant amount of Al was found in wood specimen no. 8.

For wood specimen no. 8, the case of low C_{MC} , very large cutting edge recessions were observed, VB_{OF} , VB_{OW} , and VB_{OS} . It is worth mentioning that for milling wood specimen no. 8 the cutting tool with the largest initial recessions was used. Low content of the C_{MC} also related, to a lesser degree, to wood specimens nos. 1, 2, 4, 6, and 7, for which the cutting edge recessions were found to be much smaller. The cutting edge recessions and the C_{MC} did not follow each other, although in the case of wood specimens no. 3 and 9 they did. The D differs from 395 kg/m^3 to 1,030 kg/m^3 (Table 1), but the cutting edge recessions and the D did not follow each other, especially for wood specimens nos. 3 and 9. Also wood specimen no. 7 (Kempas) had the maximum of the CS , the MOR , and the E for which the cutting edge recessions was not large. This observation suggests that the role of these mechanical wood properties in the cutting edge wearing was entangled with no clear tendency. In connection with that, in the present study, the multi-parameters theoretical simulation was performed, to separate the influence of examined parameters on the increase of cutting edge recessions: the ΔVB_F , the ΔVB_W , and the ΔVB_S , as well as verifying the methods of evaluation of the HTTR quantifiers (R_{MX} , R_{MI} , R_{Xs} , R_{Ws} , R_{As} , R_{Ss}). In the theoretical simulation, the evaluated initial cutting edge recessions (VB_{OF} ,

VB_{0W} , VB_{0S}) were employed. Earlier attempts at such multi-parameters theoretical simulation were unsuccessful, probably due to unknown problems with the TGA and the use of an average value of the VB_0 . The best approximations for observed cutting edge recessions increase were obtained when the R_{As} quantifier was employed. This suggests that the corrosion peaks for the three temperature ranges taken into account for the evaluation of the R_{As} quantifier play a reasonable role in the HSS cutting edge wearing process. The plots shown in Figs. 8 through 10 were created for the HMC particles only of fraction f_1 , minimum and average initial recessions VB_0 and the cutting path length, $C_P = 10,000$ m.

The ranges of variation of the other independent variables, the D , the C_{MC} , and the R_{As} , were reduced in order not to exceed maximum value of observed variable, VB^O . Results of theoretical simulations show (Fig. 8) that for minimum values of the initial cutting edge recession, VB_{0F} , contribution of the R_{As} quantifier cannot be seen, and maximum values of the ΔVB_F for assumed maximum values of independent variables, reached 69 μm . For the average value of the initial cutting edge recession, VB_{0F} , the contribution of the R_{As} , the C_{MC} , and the D , in an increase of the cutting edge recession measured on the clearance surface, ΔVB_F , starts from about $D = 690$ $\text{kg}\cdot\text{m}^{-3}$ and $C_{MC} = 7800$ $\text{mg}\cdot\text{kg}^{-1}$. Below these limits the influence of both the D and the C_{MC} on the VB_F is low. For the maximum value of the ΔVB_F , a synergistic effect took place of the R_{As} , and the mechanical wearing was as large as 54%. This means that all of these three independent variables separately have very low influence on the ΔVB_F .

For the minimum value of the $R_{As} = 1.36$, the largest ΔVB_F decreased by half. Calculations results for the ΔVB_W (Fig. 9), in direction of bisector of the wedge angle show much lower contributions of all independent variables in the cutting edge wearing mechanism. For the minimum values of the VB_{0W} , the ΔVB_W reached a maximum value of 37 μm , and the contribution of the R_{As} in the cutting edge wearing can be seen only for larger values of the C_{MC} and the D , when the ΔVB_W exceeds about 10 μm , at which point the influence of the C_{MC} and the D also increases. For the average value of the VB_{0W} , the ΔVB_W reached a maximum value of 43 μm . In this case there was a synergistic effect of the HTTR. The mechanical wearing was as large as 13%, which was much lower than in case of the ΔVB_F .

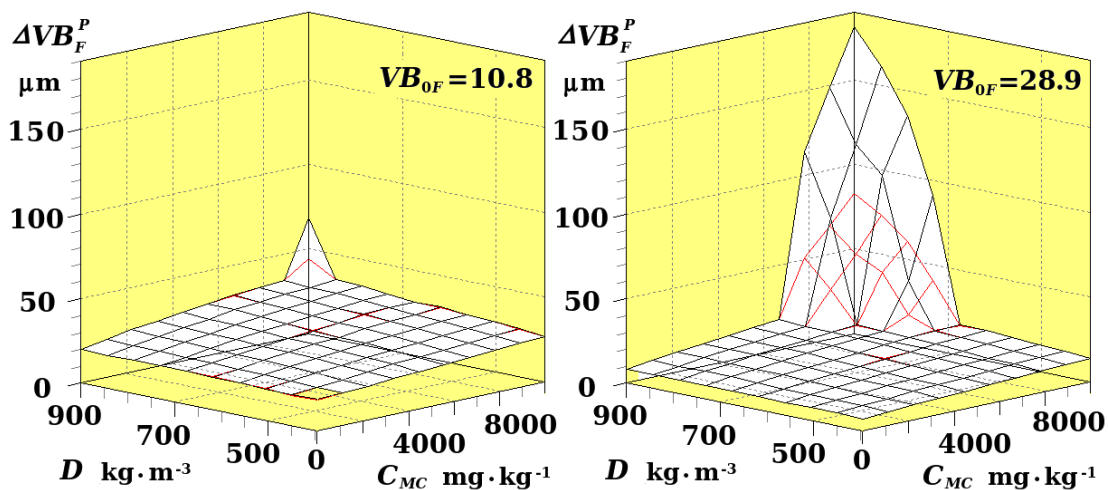


Fig. 8. Plot of observed VB_{0F} cutting edge recession, versus predicted one, VB_{0F}^P obtained from theoretical simulation; black line: $R_{As} = 2.32$, red line: $R_{As} = 1.36$

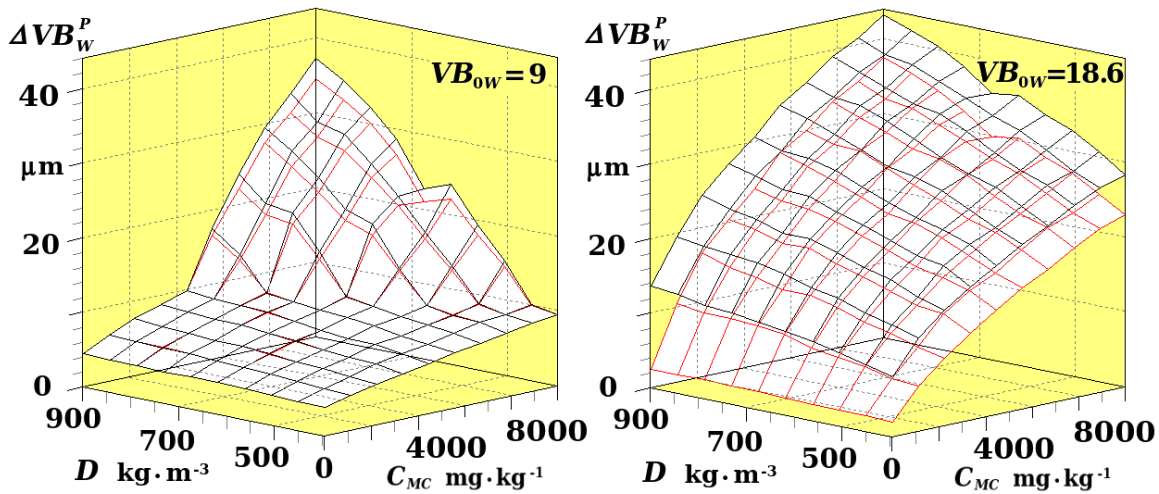


Fig. 9. Plot of observed ΔVB_W^O cutting edge recession, versus predicted one, ΔVB_W^P obtained from theoretical simulation; black line: $R_{As} = 2.32$, red line: $R_{As} = 1.36$

Results of calculations for the ΔVB_S (Fig. 10) show also low contribution of all independent variables in comparison to the ΔVB_F . Calculations performed for minimum values of the initial cutting edge recession (VB_{0S}) show that maximum values of the ΔVB_S for assumed maximum values of independent variables reached ΔVB_S equal to 15.3 μm , with almost no effect of the R_{As} , and very small influence of the C_{MC} and the D . For average value of the $VB_{0S} = 24 \mu\text{m}$, the ΔVB_W reached maximum value of 61 μm , and in this case, there was a synergistic effect of the HTTR and the mechanical wearing as large as 56%, similar to the ΔVB_F .

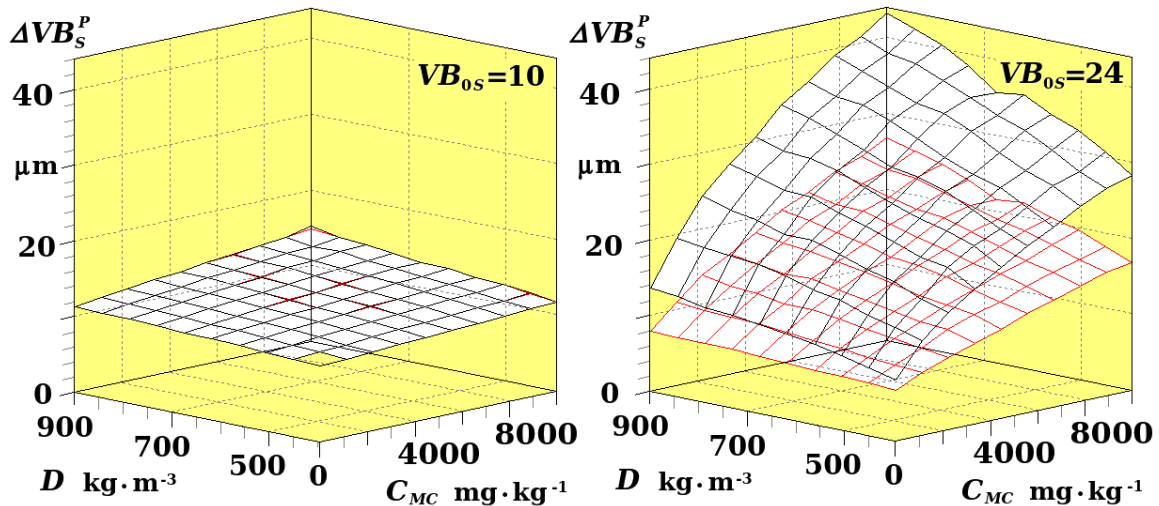


Fig. 10. Plot of observed ΔVB_S^O cutting edge recession, versus predicted one ΔVB_S^P obtained from theoretical simulation; black line: $R_{As} = 2.32$, red line: $R_{As} = 1.36$

Reduction as high as 62%, 19%, and 75% of the maximum value of respectively the ΔVB_F , the ΔVB_W , and the ΔVB_S was observed, when the VB_0 was assumed as minimum. This observation confirms a very important role of the reduction of the initial edge recessions in the reshaping process. In case of minimum of the VB_0 the role of

the R_{As} in the HSS cutting edge wearing process was almost eliminated. Results of calculations also show that the mechanism of increase of the three analyzed recessions is different. There was a successful attempt to evaluate a theoretical model of the cutting edge recessions when milling wood originating from the rain forests of Indonesia and Japan; however, it is very complicated, so more experiments should be performed in order to get better descriptions of the examined relations. Theoretical simulations that were performed with the CS , the MOR , and the E added to the experimental matrix did not allow to improve the quality of approximation of examined process.

CONCLUSIONS

There was a synergistic effect of the mechanical (caused by the C_{MC} and the D) and the chemical (caused by the $HTTR$) factors for cutting edge recession, which increased for ΔVB_F , ΔVB_W , and ΔVB_S , as high as 54%, 13%, and 56%, for the maximum values of the C_{MC} and the D .

1. At the minimum values of the VB_0 there was a significant reduction of the increase of the cutting edge recessions on clearance and rake surfaces.
2. The best approximation obtained for the R_{As} quantifier suggest that corrosion peaks for the three temperature ranges taken into account play a reasonable role in the HSS cutting edge wearing process.
3. The separate influence of analyzed independent variables (the R_{As} , the C_{MC} , and the D_F) at minimum values of the others was low.

ACKNOWLEDGMENTS

The authors are grateful for the support of the Poznań Networking & Supercomputing Center (PCSS) for a calculation grant.

REFERENCES CITED

- Amos, G. L. (1952). *Silica in Timbers*, CSIRO, Clayton, Australia, No. 267.
- Cristóvão, L., Grönlund, G., Ekevad, M., Siteo, R., and Marklund, B. (2009). "Brittleness of cutting tools when cutting Ironwood," in: *Proc. 19th Int. Wood Mach. Sem.*, Nanjing, China.
- Cristóvão, L., Lhate, I., Grönlund, A., Ekevad, M., and Siteo, R. (2011). "Tool wear for lesser-known tropical wood species," *Wood Material Science and Engineering* 6(3), 155-161. DOI: 10.1080/17480272.2011.566355.
- Porankiewicz, B. (2003a). "A method to evaluate the chemical properties of particle board to anticipate and minimize cutting tool wear," *Wood Science & Technology* 37, 47-58. DOI: 10.1007/s00226-003-0166-8.
- Porankiewicz, B. (2003b). *Tępienie się ostrzy i jakość przedmiotu obrabianego w skrawaniu płyt wiórowych* ("Cutting edge wearing and machining quality by particle board milling"). Printing House, Agricultural University of Poznań, No. 341 (in

Polish).

- Porankiewicz, B. (2006). "Theoretical simulation of cutting edge wearing when secondary wood products cutting," *Wood Science & Technology* 40, 107-117.
- Porankiewicz, B., Sandak, J., and Tanaka, C. (2005). "Factors influencing steel tool wear when milling wood," *Wood Science & Technology* 39(3), 225-234. DOI: 10.1007/s00226-004-0282-0.
- Porankiewicz, B., Iskra, P., Sandak, J., Tanaka, C., and Józwiak, K. (2006). "High speed steel tool wear after wood cutting in presence of high temperature and mineral contamination," *Wood Science & Technology* 40, 673-682. DOI: 10.1007/s00226-006-0084-7.
- Porankiewicz, B., Iskra, P., Józwiak, K., Tanaka, C., and Zborowski, W. (2008). "High speed steel tool wear after wood milling in presence high temperature tribochemical reactions," *BioResources* 3(3), 838-859. DOI: 10.15376/biores.3.3.838-858

Article submitted: January 17, 2018; Peer review completed: March 17, 2018; Revised version received: March 20, 2018; Accepted: April 2, 2018; Published: April 17, 2018.
DOI: 10.15376/biores.13.2.3892-3904

APPENDIX

The following estimators for Eqs. 7 to 31, for the ΔVB_F , were evaluated: $e_1=105.80111$; $e_2=0.1914$; $e_3=0.87242$; $e_4=1.81659$; $e_5=-5.98367 \cdot 10^{-2}$; $e_6=47.29786$; $e_7=0.5611$; $e_8=8.10204$; $e_9=3.27943$; $e_{10}=17.64729$; $e_{11}=0.39162$; $e_{12}=9.94742 \cdot 10^{-6}$; $e_{13}=1.05509 \cdot 10^{-6}$; $e_{14}=1.23453 \cdot 10^{-7}$; $e_{15}=6.977 \cdot 10^{-9}$; $e_{16}=7.86738 \cdot 10^{-2}$; $e_{17}=6.84019 \cdot 10^{-2}$; $e_{18}=9.58575 \cdot 10^{-6}$; $e_{19}=9.98129 \cdot 10^{-7}$; $e_{20}=1.30198 \cdot 10^{-7}$; $e_{21}=8.179 \cdot 10^{-9}$; $e_{22}=0.838$; $e_{23}=0.32098$; $e_{24}=0.27857$; and $e_{25}=8.1909 \cdot 10^{-2}$, by summation of square of residuals as high as $S_K=729.5$, correlation coefficient between predicted the observed recessions as high as $R=0.998$ and the standard deviation $S_D=9.1$.

The following estimators for Eqs. 7 to 31, for the ΔVB_W , were evaluated: $e_1=12.4821$; $e_2=0.18063$; $e_3=0.58194$; $e_4=1.67074$; $e_5=-3.69965 \cdot 10^{-2}$; $e_6=19.8861$; $e_7=0.22358$; $e_8=5.90069$; $e_9=0.15666$; $e_{10}=10.64828$; $e_{11}=2.09201$; $e_{12}=1 \cdot 10^{-5}$; $e_{13}=9.5323 \cdot 10^{-7}$; $e_{14}=1.07756 \cdot 10^{-7}$; $e_{15}=1 \cdot 10^{-8}$; $e_{16}=1.59231 \cdot 10^{-2}$; $e_{17}=36.34688$; $e_{18}=1 \cdot 10^{-5}$; $e_{19}=1 \cdot 10^{-6}$; $e_{20}=1 \cdot 10^{-7}$; $e_{21}=1 \cdot 10^{-8}$; $e_{22}=0.75586$; $e_{23}=0.29782$; $e_{24}=0.15707$; and $e_{25}=7.38522 \cdot 10^{-2}$; by: the $S_K=338.6$, the $R=0.989$ and $S_D=6.4$.

The following estimators for Eqs. 7 to 31, for the ΔVB_S , were evaluated: $e_1=11.91796$; $e_2=0.34643$; $e_3=0.34349$; $e_4=1.59324$; $e_5=-2.2916 \cdot 10^{-2}$; $e_6=24.88184$; $e_7=0.32224$; $e_8=3.31983$; $e_9=2.94091$; $e_{10}=5.14568$; $e_{11}=1.21621$; $e_{12}=10^{-5}$; $e_{13}=7.52823 \cdot 10^{-7}$; $e_{14}=9.4074 \cdot 10^{-8}$; $e_{15}=1.0217 \cdot 10^{-8}$; $e_{16}=1.16367 \cdot 10^{-2}$; $e_{17}=23.35736$; $e_{18}=9.32246 \cdot 10^{-6}$; $e_{19}=7.05635 \cdot 10^{-7}$; $e_{20}=1.25084 \cdot 10^{-7}$; $e_{21}=8.34710^{-9}$; $e_{22}=1.14348$; $e_{23}=0.28774$; $e_{24}=6.83483 \cdot 10^{-2}$; and $e_{25}=5.53764 \cdot 10^{-2}$; by: $S_K=204.2$, the $R=0.989$ and the $S_D=5.1$.